Doping effect on nanoscopic and macroscopic electrical properties of Barium Zirconate Titanate thin films

Amina Tachafine, Didier Fasquelle, Rachel Desfeux, Anthony Ferri, A. da Costa, Jean-Claude Carru, A. Outzourhit

Doping effect on nanoscopic and macroscopic electrical properties of Barium Zirconate Titanate thin films

Short title: **Barium Zirconate Titanate thin films properties**

A. Tachafine [a], D. Fasquelle [a], R. Desfeux [b], A. Ferri [b], A. Da Costa [b], J.-C. Carru [a], A. Outzourhit [c]

[a] *Unité de Dynamique et Structure des Matériaux Moléculaires, Université du Littoral - Côte d'Opale, 50 rue Ferdinand Buisson, B.P. 717, 62228 Calais, France.*

[b] *Univ. Artois, CNRS, Centrale Lille, Univ. Lille, UMR 8181, Unité de Catalyse et Chimie du Solide (UCCS), F-62300 Lens, France*

[c] *Nanomaterials Laboratory for Energy and Environment, Department of Physics, Faculty Semlalia, Cadi Ayyad University, Marrakech, BP 2390, 40000, Morocco*

tachafin@univ-littoral.fr

Abstract

Lead-free Barium Zirconate Titanate thin films synthesized by sol-gel process were deposited on platinized silicon substrates. Atomic and piezoresponse force microscopies analysis have revealed low values for the surface roughness and local piezoelectric loops, respectively. Nanoscopic piezoelectric and ferroelectric properties decrease with zirconium content increasing. Dielectric measurements were made up to 1 MHz at room temperature. The highest dielectric permittivity and tunability are obtained for 10% of zirconium. Dielectric loss tangent decreases with frequency, zirconium content and electric field increasing. Thin films with 20% of zirconium could be particularly interesting for electronic applications.

Keywords: Barium Zirconate Titanate, thin film, nanoscale investigations, dielectric measurements, atomic force microscopy, piezoresponse force microscopy

1-Introduction

Ferroelectric materials have enabled significant technological advances in electronics in recent years. The development of components such as resonators, capacitors, sensors, memories, or tunable microwave devices, has contributed significantly to innovating in computing, microelectronics and telecommunications in both the military and civilian fields [1-3]. Fundamental and applied research in materials is therefore an important objective for the future. The aim of this work is to realize and optimize frequency tunable systems for electronic applications. In this view, the simplest structure is capacitor tunable with continuous voltage that can be afterwards integrated in tunable or reconfigurable high frequency devices such as high frequency filters or resonators [4-5]. In this sense, thin films derived from the barium titanate ($BaTiO_3$) ferroelectric material still generate a lot of work for the development of integrated components for microelectronics such as flat capacitors, coplanar waveguides or tunable filters [6]. Indeed, $BaTiO_3$ has good dielectric properties, which make it the most used base material to elaborate high dielectric permittivity capacitors [7]. In particular, the lead-free environmentally friendly barium zirconate Titanate $BaZr_xTi_{1-x}O_3$ (BZT) material obtained by substituting $BaTiO_3$ at B sites with zirconium has been suggested as an alternative to the barium strontium Titanate $Ba_{1-x}Sr_xTiO_3$ (BST) material for the fabrication of capacitors, because zirconium ion Zr^{4+} is chemically more stable than titanate ion Ti^{4+} [8–10]. Additionally, the relatively large dielectric loss and the limited figure of merit (FOM) of BST restrict the practical applications in tunable microwave devices [11]. The interest of the BZT material lies in the fact that it has a high dielectric permittivity, low dielectric losses and a high tunability of the dielectric permittivity [11]. Moreover, depending on the zirconium content, this material presents different dielectric properties because it can exhibit either a classical ferroelectric or

relaxor behavior [12]. This material offers opportunities for the development of various microwave devices such as tunable filters, resonators, phase shifters and microstrip lines and so on. For the improvement of the dielectric properties of BZT thin films, different methods of elaboration have been used: Chemical solution deposition [13], sputtering [14], pulsed laser deposition (PLD) [15], sol-gel [16], hydrothermal techniques [17] and recently plasma electrolyte oxidation [18]. Various works of the literature have focused on the choice of the substrate [19], optimizing deposition parameters [20], doping [21], buffer layer insertion [22].

Works on BZT thin film synthesis continue to draw the interest of the scientific community as evidenced by recent works in the literature, such as the deposition of $BaZr_{0.35}Ti_{0.65}O_3$ thin film by radio frequency magnetron sputtering technique for making capacitors with high energy storage density [23]. It can be also mention the development of lead-free nanogenerators in the conversion of mechanical energy with the $Ba(Zr_{0.2}Ti_{0.8})O_3$-$x(Ba_{0.7}Ca_{0.3})TiO_3$ (BZT-xBCT) system which shows impressive piezoelectric properties (d_{33} ~ 620 pC/N) because they are comparable to those of the lead zirconate $PbZrO_3$ conventional material [24-26]. These results position the BZT-xBCT system as a serious alternative to lead-based piezoelectrics and pave the way for investigations of this lead-free ferroelectric system for other compositions and synthesis methods. [27].

In addition, with the development of nanotechnologies, current miniaturization requirements lead to the reduction of the size of components to dimensions below one micron. This has led to a strong interest in size effects and studies of the local ferroelectric and piezoelectric properties of materials. Non-destructive atomic force microscopy (AFM) and piezoresponse force microscopy (PFM) measurements allow access to the local piezoelectric and ferroelectric properties and to the architecture of ferroelectric domains with high resolution [28].

This work is a contribution to the development and study of lead-free materials for electronic applications. $BaZr_xTi_{1-x}O_3$ thin films have been synthesized by sol-gel process with x varying

from 0 ($BaTiO_3$) to 0.35 by step of 5%. Electrical characterizations were also done as a function of ziconium content at both the nanoscopic and macroscopic scales. Actually, AFM and PFM analysis were used for revealing the surface properties and local hysteresis loops, respectively. Moreover, dielectric measurements with and without bias were done for the study of the dielectric constant, losses, loss tangent and tunability.

2-Experimental procedure

$BaZr_xTi_{1-x}O_3$ solutions with x=0 to 0.35 with a 5% step were prepared by sol-gel process [29] using barium acetate ($C_4H_6BaO_4$), zirconium (IV)-butoxide ($Zr[O(CH_2)_3]_4$), and Titanium (IV) n-butoxide ($C_{16}H_{36}O_4Ti$) as starting materials. BZT films were deposited onto platinized silicon substrates by spin coating. Crystallization was achieved via post-deposition annealing at 750°C for 1 hour for all the samples. To determine the electrical properties, metallic electrodes were deposited on BZT films: gold has been evaporated through a shadow mask to realize the upper electrode with circular patches ranging from 150 µm to 500 µm in diameter. The film thickness was measured with a Talysurf intra 150 profilometer and is of about 500 nm. Electrical properties were determined at room temperature in the frequency range 10^2-10^6 as function of the DC bias (-10 V, +10 V) with an Agilent HP4284A impedance analyser coupled to low frequency Cu/Be microprobes.

For nanoscopic measurements, a commercial atomic force microscope (AFM) (Multimode, Nanoscope IIIa, Bruker) working under environmental conditions was used for both surface morphology and local piezoelectric response of the BZT thin films. For topography imaging, AFM measurements were performed in the contact mode with micro-fabricated Si_3N_4 cantilevers and Si ultralever tips using a small repulsion force [30-31]. For domain imaging, piezoelectric response of the surface which form is $A\cos\varphi$ (the amplitude A defines the local electromechanical response, the phase φ yields information on the polarization direction below the tip) was carried out using platinum/iridium coated silicon tip with spring constants of 0.2

N/m [32]. For measurements of local piezoelectric hysteresis loops, the spectroscopic tool of PFM was used. The applied DC voltage was gradually swept from +10 V down to -10 V then from -10 V up to +10 V within a period of 200 s. The frequency and the amplitude of the driving AC voltage were f = 2 kHz and V_{ac} = 1.5 V, respectively. The piezoloops were obtained by plotting the phase and the amplitude as a function of the DC voltage. The phase and amplitude hysteresis loops were recorded simultaneously for each probed grain.

3-Results and discussions

3-1 Nanoscopic properties

3-1-1 Atomic force microscopy measurements

Surface roughness is an important parameter in the production of thin film dielectric capacitors since dielectric properties depend not only on the microstructure of the thin film but also on the interface between the electrode and the dielectric material. This interface strongly influences parameters such as the leakage current and the breaking electric field of the thin film [33]. Roughness is also an important parameter in multilayer systems where dielectric properties are strongly influenced by the mismatch at the interfaces between alternating layers of different materials. Figure 1 shows AFM images from 2 μm x 2 μm BZT thin films for x=0, 0.05, 0.15, 0.25 and 0.35. These images taken on the surface of the films show that the films are all granular with clear differences between the morphologies of their surfaces. The root mean square (RMS) roughness values measured over 20 x 20 μm^2 scan areas decrease as the zirconium content increases: from 6.0 nm for the $BaTiO_3$ film to 1.4 nm for the BZT0.35 film. The decrease in RMS roughness with increase in zirconium content seems to be associated to the slow diffusion of the Zr^{4+} ion (0.087 nm), which has a larger ionic radius than Ti^{4+} (0.068 nm). Indeed, it is well known that barium zirconate ($BaZrO_3$) is a difficult refractory oxide (T_{fusion} =2600 °C), which leads to a gradual decrease in grain size as the zirconium content in the material increases. The morphology of these films is therefore strongly dependent on the zirconium composition.

It can be also note that as a first approximation, the measured BZT thin films roughness is almost linear as a function of zirconium content starting from x=0.15 (figure 2). Values of surface roughness can then be controlled by adjusting the Ti/Zr ratio. For comparison, the RMS roughness value obtained for x=0.1 (2.5 nm) is significantly lower than that (10 nm) obtained for a $BaZr_{0.1}Ti_{0.9}O_3$ thin film synthesized using the RF magnetron sputtering system [11]. This would be in favor of a smaller interfacial layer between the ferroelectric material and the lower electrode in the thin film. This should also be favorable for the realization of multilayer capacitors with BZT films synthesized by sol-gel process.

3-1-2 Piezoresponse hysteresis loops

Figure 3 presents local piezoelectric hysteresis phase-recorded loops at the surface of a grain with an average diameter of about 50 nm for BZT thin films with x=0.05 (a), x=0.15 (b), x=0.25 (c) and x=0.35 (d). During these measurements, the tip has been placed at the center of the grain to avoid grain boundaries contributions. All the BZT compositions studied respond well to the excitation of the applied electric field and well-defined hysteresis loops are obtained. For these zirconium contents ($0 \leq x \leq 0.35$), local piezoelectric phase responses degrade depending on the increasing zirconium content: from 140° for x=0.05 to 120° for x=0.35 for phase difference. Moreover, the cycles become more and more inclined as the zirconium rate increases, in accordance with the paraelectric state of the material at room temperature for high zirconium rates ($x \geq 0.35$).

Measured coercive voltages ($2V_c=V_{c1}-V_{c2}$) are of 3.2 V, 2.5 V, 2.8 V and 2.0 V for compositions x=0.05, 0.15, 0.25 and 0.35, respectively. The phase responses of BZT thin films show a shift towards the positive or negative values of the applied voltage. This asymmetry is usually attributed to an internal electric field at the interface between the platinum electrode and the BZT layer and/or to the heterostructure of the tip/film/electrode system, which provides its own asymmetry [34-37]. This is because charges could fill band gap states in films near the

surface where the tip is located or at the lower film/electrode interface. In particular, electrons trapped in these bandgap states would form a negative spatial charge near the film surface, leading to the voltage shift observed over the loops [28].

Figure 4 shows local amplitude loops simultaneously recorded at the center of individual grains of BZT thin films with x=0.05 (a), x=0.15 (b), x=0.25 (c) and x=0.35 (d) thin films. As the signal comes from a synchronous detection, the amplitude of the signal is in absolute value and the phase gives information about the direction of the mechanical variation of the grain. A memory effect, linked to the ferroelectric character is recovered which gives the signal its butterfly-winged appearance. These results confirm the ferroelectric and piezoelectric character of BZT grains. Curves clearly show a mechanical deformation in the grain under a DC voltage owing the converse piezoelectric effect. This effect decreases with increasing zirconium content as shown by the decrease in the total measured amplitude from 0.8 mV for x=0.05 to 0.25 mV for x=0.35. The BZT thin films piezoelectric character decreases then with increasing zirconium content in the composition, but it is still present for x=0.35.

If it can be estimated that at zero voltage there is no mechanical movement of the grain, a relative variation in the amplitude and therefore in the piezoelectric activity of the grain is observed. For example, this variation is more than 100 % for the BZT film with 35% of Zirconium under a positive voltage of 10 volts. It can be observed that the amplitude variation is slightly different for positive and negative polarization. This may be due to the interface effect and/or the instrumental electrostatic contribution, which is quite common in such devices. [28].

Acosφ piezoelectric response (Figures 5-a and 5-b) show typical piezoelectric loops of a ferroelectric material for BZT thin films with x<0.25. The width of the loops decreases as the zirconium content increases. For x=0.25, the hysteresis loop is barely open, which shows that the ferroelectric to paraelectric transition of this film is very close to room temperature, at which

the measurements were made. During the acquisition of a local piezoelectric loop, the measurement is well localized on the surface of the sample using a tip (analyzed surface ~ $\pi.30^2$ nm^2, 30 nm corresponding to the tip's apex). Nanoscale analysis then only provides information on the area below the tip. Thus in our case it is noticed that the analyzed domain presents an asymmetric piezoelectric loop where the negative part is less pronounced than the positive part. However, it should be noted that this piezoresponse loop is saturated both for positive polarization from 7 V and from -5 V for negative polarization.

3-2 Macroscopic properties

3-2-1 Dielectric measurements without DC polarization

Figure 6 shows the frequency dependence of BZT thin films dielectric permittivity in the range [1 kHz-1 MHz] at room temperature. The dielectric permittivity is derived from the capacitance measurement of the parallel electrical model of the Metal-Insulator-Metal (MIM) structure and after measuring the film thickness. The relative dispersion of the dielectric permittivity, given by Equation 1, is between 7% and 13% for all the studied BZT compositions. This dispersion is due to oxygen gaps, BZT film-electrode interfaces and impurities and mainly attributed to the dipoles that could not follow the rapidly alternation of the electric field in the whole frequency range [38].

$$Relative\ dispersion = \frac{\varepsilon'(1\ \mathrm{kHz}) - \varepsilon'(1\ \mathrm{MHz})}{\varepsilon'(1\ \mathrm{kHz})} \quad (1)$$

The evolution of the dielectric permittivity as a function of the zirconium content at 1 MHz and room temperature is shown in Figure 7. The dielectric constant increases and passes through a maximum for a zirconium content of 10% and then gradually decreases with the zirconium content increasing. Similar results were obtained for BZT thin films synthesized by soft chemical spin-coating technique, rf magnetron sputtering or metalorganic chemical vapor deposition (MOCVD) [39]. Indeed, in BZT material, paraelectric-ferroelectric, quadratic-orthorhombic and orthorhombic-rhombohedral transition temperatures become confused at

about 280 K, i.e. close to room temperature, for a zirconium content of 10%. At higher zirconium contents, the paraelectric-ferroelectric transition temperature decreases, resulting in a decrease in dielectric permittivity [40]. Additionally, at the nanoscopic scale (figure 2) an increase in zirconium content induces a reduction in RMS roughness, which suggest that Zr^{4+} ions can decrease dielectric permittivity.

The dielectric loss tangent tgδ (Figure 8) gradually decreases with frequency increasing, except for x=0.05. This decrease is due to the space charge polarization effect when frequency is below 1 MHz [41-42]. Indeed, space charge polarization is related to the macroscopic movement of charge carriers easily captured by defects, impurity, phase boundary, and so on. Mobile charge carriers are then impeded by the grain boundary that is a physical barrier inhibiting charge migration. The charges pile up at the barrier, producing a localized polarization within grains. It should be noted a slight dielectric relaxation for x=0.1 and x=0.2. For x=0.05, dielectric measurements beyond 1 MHz are required to confirm possible dielectric relaxation.

As a comparison for x=0.2, a tgδ value of $1.8\ 10^{-2}$ at 1 MHz is obtained. This value is 5 times lower than the one obtained recently (0.093) by Guo et al. for a BZT thin film of the same composition and synthesized by sol-gel process [43].

Figure 9 shows the evolutions of the dielectric losses (ε'') and loss tangent (tgδ) as a function of the zirconium content at 1 MHz and room temperature. Dielectric losses evolve in the same way as the dielectric constant: they increase and go through a maximum for a zirconium rate of 10% and then decrease. It is interesting to notice the continuous decrease of the dielectric loss tangent with the zirconium content increasing: $tg\delta_{min} = 1.4\ 10^{-2}$ for x=0.35 at 1 MHz. If the dielectric loss tangent continues to decrease beyond 1 MHz, this composition would be interesting for radiofrequency and microwave applications. It would also be interesting to carry out similar investigations on BZT thin films with zirconium contents higher than 0.35.

3-2-2 Dielectric measurements with DC polarization

Figure 10 shows the evolution of the BZT thin films dielectric permittivity as a function of the applied electric field at 1 MHz and room temperature. The electric field was applied from -250 kV/cm to +250 kV/cm. There is a "butterfly wing" shape characteristic of ferroelectric behavior, indicating the strong ferroelectric property of BZT thin films. The evolution of the dielectric permittivity depends strongly on the zirconium content: it remains higher for x=0.1 and the hysteresis effect is even more attenuated with the zirconium content increasing. Nevertheless, the "butterfly-wing" shape is still present up to x=0.35. These macroscopic results are in perfect agreement with the nanoscopic measurements carried out at the level of a grain (Figure 3, 4 and 5). In addition, the dielectric permittivity evolutions are not symmetrical with respect to the vertical axis at 0 V/cm. This effect may stem from various causes such as the different nature of the planar capacitor electrodes, since the lower electrode is made of platinum while the upper electrode is made of gold, or interface effects between the different thin films layers, or the distribution and/or generation of space charges created by the electric field. Dielectric losses (figure 11) follow the same evolution as the dielectric permittivity. The dielectric losses nonlinearly decrease with the electric field increasing, which can be attributed to the anharmonic interaction of Ti ions at the paraelectric phase [44]. This decrease with the electric field increasing is particularly interesting for applications and shows that such samples have a very good resistance to breakdown.

Figure 12 shows the BZT thin films tunability as a function of the applied electric field from -250 kV/cm to +250 kV/cm at 1 MHz and room temperature. The highest tunability is achieved for the BZT0.1 thin film. Indeed, the highest tunability is obtained at the ferroelectric-to-paraelectric phase transition. When the material is in the paraelectric state but at a temperature far from the Curie temperature, no tunability is observed [45]. The evolution of tunability as a function of the zirconium content for an applied electric field of 240 kV/cm at 1 MHz and room temperature is shown in Figure 13. The measured tunability is of 11% for the $BaTiO_3$ thin film.

It increases with the zirconium content increasing, passes through a maximum of 32% for x=0.1, then decreases to reach 17.5% for x=0.35. It is known that the quality of a material depends not only on its tunability but also on the losses, which must be as low as possible. A figure of merit (FOM), taking into account the relationship between these two quantities, is defined by Equation 2.

$$FOM = \frac{Tunability}{\text{tg}\delta\ (\%)} \quad (2)$$

The higher the FOM factor, the more advantageous the sample characteristics are for applications requiring high dielectric permittivity tunability. FOM calculations display a maximum value of 15 for x=0.2 at 240 kV/cm and room temperature. This composition could therefore be used for frequency agility electronics applications.

4-Conclusion

$BaZr_xTi_{1-x}O_3$ (x=0, 0.05, 0.1, 0.15, 0.2, 0.25 and 0.35) thin films with a typical thickness of 0.5 μm were deposited via sol–gel process on platinized silicon substrates. AFM analyses showed homogenous and dense microstructures for all the $BaZr_xTi_{1-x}O_3$ thin films and low values for the surface roughness decreasing with the zirconium content increasing, from 6.0 nm for x=0 to 1.4 nm for x=0.35. This shows the interest of the sol-gel process, known as "soft chemistry", which has the additional advantage of being very inexpensive. Electric characterizations were performed on BZT films at both the nanoscopic and macroscopic levels. On the nanoscale level, local piezoelectric hysteresis phase- and amplitude-recorded loops at the surface of a grain with an average length of about 50 nm were produced by PFM over the center of the grain. They have evidenced the ferroelectric and piezoelectric character of BZT thin films grains at the nanoscopic scale, showing that ferroelectricity exists at dimensions of the order of 50 nm. PFM measurements showed a decrease in local responses with the zirconium content increasing. These qualitative piezoelectric results are very encouraging for lead-free piezoelectric applications.

On the macroscopic level, dielectric measurements carried out on BZT thin films up to 1 MHz at room temperature confirmed the observed ferroelectric properties at the grain level. Every film studied displays a non-linear variation in dielectric permittivity and losses as a function of the applied DC electrical field. The BZT thin films' dielectric permittivity and tunability are maximal for x=0.1 and decrease with the zirconium content increasing. The dielectric loss tangent tgδ gradually decreases with frequency and the zirconium content increasing. Dielectric losses decrease with the electric field increasing, which is particularly interesting for applications and shows a very good resistance to breakdown.

FOM calculations show that the $BaZr_{0.2}Ti_{0.8}O_3$ thin film is of great interest for the development of monolithic ceramic capacitors dedicated to radiofrequency and microwave electronic applications. This work is part of an international context that aims to exploit the physical properties of ferroelectric materials in the field of telecommunications in order to finalize an application such as that of tunable capacitors.

Acknowledgement

The authors thank L. Maës for technical support. Chevreul Institute (FR 2638), Ministère de l'Enseignement Supérieur, de la Recherche et de l'Innovation, Hauts-de-France Region, Fonds Européen de Développement Régional (FEDER) and Major Domain of Interest (DIM) "Eco-Energy Efficiency" of Artois University are acknowledged for supporting and funding partially this work.

References

[1] Burgnies, L.; Vélu, G.; Blary, K.; Carru, J.-C. ; Lippens, D. Tunability of ferroelectric varactors uo to 60 GHz. *Electronics Letters* **2007**, 43, 1151-1152.

[2] Jeon, J.H. Effect of $SrTiO_3$ concentration and sintering temperature on microstructure and dielectric constant of $Ba_{1-x}Sr_xTiO_3$. *Journal of the European Ceramic Society* **2004**, 24, 1045-1048.

[3] Takasu, J. H. The ferroelectric memory and its applications. Journal of Electroceramics **2000**, 4, 327-328.

[4] Outzourhit, A.; Trefny, J.U. Tunability of the dielectric constant of $Ba_{0.1}Sr_{0.9}TiO_3$ ceramics in the paraelectric state. Journal of Material Research Society **1995**, 10 (6), 1411-1417.

[5] Wu, L.; Chen, Y.-C.; Chen, L.-J.; Chou, Y.-P.; Tsai, Y.-T. Preparation and Microwave Characterization of $Ba_xSr_{1-x}TiO_3$ Ceramics. *Japanese Journal of Applied Physics* **1999**, 38 (9B), 5612-5615.

[6] Curecheriu, L.P.; Tufescu, F.M.; Ianculescu, A.; Ciomaga, C.E.; Mitoseriu, L.; Stancu, A. Tunability characteristics of BaTiO3 – based ceramics: Modeling and experimental study. *Journal of optoelectronics and advanced materials* **2008**, 10 (7)**,** 1792 – 1795.

[7] Tagantsev, A.K.; Sherman, V.O.; Astafiev, K.F.; Venkatesh, J.; Setter, N. Ferroelectric materials for microwave tunable applications. *Journal of Electroceramics* **2003**, 11, 5-66.

[8] Rehrig, P.W.; Park, S.-E.; Trolier-McKinstry, S.; Messing, G.L.; Jones, B.; Shrout, T.R. Piezoelectric properties of zirconium-doped barium titanate single crystals grown by templated grain growth. *Journal of Applied Phys*ics **1999**, 86, 1657-1661.

[9] Yu, Z.; Guo, R.; Bhalla, A. S. Orientation dependence of the ferroelectric and piezoelectric behavior of single crystals. *Applied Phyics Letters* **2000**, 77, 1535-1537.

[10] Yu, Z.; Guo, R.; Bhalla, A. S. Dielectric behavior of single crystals. *Applied Phyics Letters* **2000**, **88**, 410-416.

[11] Chen, H.; Yang, C.; Zhang, J.; Wang, B.; Ji, H. Electrical behavior of $BaZr_{0.1}Ti_{0.9}O_3$ and $BaZr_{0.2}Ti_{0.8}O_3$ thin films. *Applied Surface Science* **2009**, 255 (8), 4585-4589.

[12] Tachafine, A.; Aoujgal, A.; Rguiti, M.; Graça, M.P.F.; Costa, L. C. ; Outzourhit, A.; Carru, J.-C. Classical and Relaxor Ferroelectric Behavior of Titanate of Barium and Zirconium Ceramics. *Spectroscopy Letters* **2014**, 47 (5), 404-410.

[13] Hofer, C.; Hoffmann, M.; Boettger, U.; Waser, R. Relaxors as High-ε-Materials for Multilayer and Thin Film Capacitors. *Ferroelectrics* **2002**, 270 (1), 179-184.

[14] Kamehara, N.; Sukada, M.T.; Cross, J.S.; Kurihara, K. J. *Journal of the Ceramic Society of Japan* **1997**, (105), 746-749.

[15] Halder, S.; Bhattacharyya, S.; Krupanidhi, S.B. Electrical characterization of $Ba(Zr_{0.1}Ti_{0.9})O_3$ thin films grown by pulsed laser ablation technique. *Materials Science and Engineering* **2002**, B 95, 124-130.

[16] Dixit, A.; Majumder, S.B.; Savvinov, A.; Katiyar, R.S.; Guo, R.; Bhalla, A.S. Investigations on the sol–gel-derived barium zirconium titanate thin films. *Materials Letters* **2002**, 56, 933-940.

[17] Alvarez, A.V.; Fuenzalida, V.M. Evidence of transition metal diffusion during hydrothermal ceramic film growth: $Ba(Ti,Zr)O_3$ on layered Ti–Zr alloy. *Journal of materials research* **1999**, 14, 4136-4139.

[18] Teng, H.-P.; Lu, F.-H. Production of $Ba(Zr,Ti)O_3$ coatings on ternary (Ti,Zr)N thin film electrodes by plasma electrolyte oxidation. *Surface and Coatings Technology* **2020**, 385, 125440.

[19] Zhu, X.H.; Li, J.; Zheng, D.N. Frequency and temperature dependence of tunable dielectric properties of $Ba(Zr_{0.2}Ti_{0.8})O_3$ thin films grown on (001) MgO. *Applied Physics Letters* **2007**, 90, 142913.

[20] Zhai, J.; Yao, X.; Zhang, L.; Shen, B. Dielectric nonlinear characteristics of $Ba(Zr_{0.35}Ti_{0.65})O_3$ thin films grown by a sol–gel process, *Applied Physics Letters* **2004**, 84, 3136-3138.

[21] Jie, W.J.; Zhu, J.; Qin, W.F.; Wei, X.H.; Xiong, J.; Zhang, Y.; Bhalla, A.; Li, Y.R. Enhanced dielectric characteristics of preferential (111)-oriented BZT thin films by manganese doping, *Journal of Physics D: Applied Physics* **2007**, 40, 2854–2857.

[22] Tang, X.G.; Tian, H.Y.; Wang, J.; Wong, K.H.; Chan, H.L.W. Effect of $CaRuO_3$ interlayer on the dielectric properties of $Ba(Zr,Ti)O_3$ thin films prepared by pulsed laser deposition, *Applied Physics Letters* **2006**, 89, 142911.

[23] Fan, Q.; Ma, C. ; Ma, C.; Lu, R.; Cheng, S.; Liu, M. Manipulating leakage behavior via thickness in epitaxial $BaZr_{0.35}Ti_{0.65}O_3$ thin film capacitors. *Applied Physics Letters* **2020**, 116, 192902.

[24] Liu, W.; Ren, X. Large Piezoelectric Effect in Pb-Free Ceramics. *Physical Review Letters* **2009**, 103, 257602.

[25] Ehmke, M.C.; Glaum, J.; Hoffman, M.; Blendell, J.E.; Bowman, K.J. In Situ X-ray Diffraction of Biased Ferroelastic Switching in Tetragonal Lead-free $(1-x)Ba(Zr_{0.2}Ti_{0.8})O_3–x(Ba_{0.7}Ca_{0.3})TiO_3$ Piezoelectrics. *Journal of the American Ceramic Society* **2013**, 96 (9), 2913–2920.

[26] Zhang, L.; Zhang, M.; Wang, L.; Zhou, C.; Zhang, Z.; Yao, Y.; Zhang, L.; Xue, D.; Lou, X.; Ren, X. Phase transitions and the piezoelectricity around morphotropic phase boundary in $Ba(Zr_{0.2}Ti_{0.8})O_3$-$x(Ba_{0.7}Ca_{0.3})TiO_3$ lead-free solid solution. *Applied Physics Letters* **2014**, 105, 162908.

[27] Taoa, Z.; Chea , F.; Hana, Y. ; Wanga, F.; Yanga, Z.; Qib, W.; Wub, Y.; Zhanga, K. Out-of-plane and In-plane piezoelectric behaviors of $[Ba(Zr_{0.2}Ti_{0.8})\ O_3]–0.5(Ba_{0.7}Ca_{0.3}TiO_3)$ thin films. *Progress in Natural Science: Materials International* **2017**, 27 (6), 664-668.

[28] Ferri, A.; Saitzek, S.; Da Costa, A.; Desfeux, R.; Leclerc, G.; Bouregba, R. ; Poullain, G. Thickness dependence of the nanoscale piezoelectric properties measured by piezoresponse

force microscopy on (111)-oriented PLZT 10/40/60 thin films. *Surface Science* **2008**, 602, 1987–1992.

[29] Velu, G.; Carru, J.-C; Cattan, E.; Remiens, D.; Melique, X.; Lippens, D. Deposition of Ferroelectric BST Thin Films by Sol Gel Route in View of Electronic Applications. *Ferroelectrics* **2003**, 288 (1), 59-69.

[30] Desfeux, R.; Da Costa, A.; Prellier, W. Thickness dependence on the surface morphology and the magnetic microstructure of $La_{0.7}Sr_{0.3}MnO_3$ films under different strains. *Surface Science* **2002**, 497 (1-3), 81-92.

[31] Desfeux, R.; Legrand, C.; Da Costa, A.; Chateigner, D.; Bouregba, R.; Poullain, G. Correlation between local hysteresis and crystallite orientation in PZT thin films deposited on Si and MgO substrates. *Surface Science* **2006**, 600, 219-228.

[32] Kalinin, S.V.; Bonnell, D.A. Imaging mechanism of piezoresponse force microscopy of ferroelectric surfaces. *Physical Review B* **2002**, 65, 125408.

[33] Oh, J.-H.; Lee, Y. H.; Ju, B.K.; Shin, D.K.; Park, C.-Y.; Oh, M.H. Impact of surface properties on the dielectric breakdown for polycrystalline and multilayered $BaTiO_3$ thin films. *Journal of Applied Physics* **1997**, 82 (12), 6203-6208.

[34] Gruverman, A.; Kholkin, A.; Kingon, A.; Tokumoto, H. Asymmetric nanoscale switching in ferroelectric thin films by scanning force microscopy. *Applied Physics Letters* **2001**, 78, 2751-2753.

[35] Shvartsman, V.V.; Kholkin, A.L.; Pertsev, N.A. Piezoelectric nonlinearity of $Pb(Zr,Ti)O_3$ thin films probed by scanning force microscopy *Applied Physics Letters* **2002**, 81, 3025-3027.

[36] Dunn, S.; Whatmore, R. Substrate effects on domain structures of PZT 30/70 sol-gel films via PiezoAFM. *Journal of the European Ceramic Society* **2002**, 22, 825–833.

[37] Gruverman, A.; Rodriguez, B.J.; Nemanich, R.J., Kingon, A.I. Nanoscale observation of photoinduced domain pinning and investigation of imprint behavior in ferroelectric thin films. *Journal of Applied Physics* **2002**, 92, 2734-2739.

[38] J. Chen, Z. Tang, Y. Bai, S. Zhao. Multiferroic and magnetoelectric properties of $BiFeO_3/Bi_4Ti_3O_{12}$ bilayer composite films. *Journal of Alloys and Compounds* **2016**, 675, 257-265.

[39] Pontes, F.M.; Escote, M.T; Escudeiro, C.C.; Leite, E.R.; Longo, E.; Chiquito, A. J.; Pizani, P.S.; Varela, J.A. Characterization of $BaTi_{1-x}Zr_xO_3$ thin films obtained by a soft chemical spin-coating technique. *Journal of applied Physics* **2004**, 96 (8), 4386-4391.

[40] Dixit, A.; Majumder, S.B.; Dobal, P.S.; Katiyar, R.S.; Bhalla, A.S. Phase transition studies of sol–gel deposited barium zirconate titanate thin films. *Thin Solid Films* **2004**, 447, 448, 284-288.

[41] Singh, K.; Baral, A.K.; Thangadurai, V. Grain boundary space charge effect and proton dynamics in chemically stable perovskite-type $Ba_{0.5}Sr_{0.5}Ce_{0.6}Zr_{0.2}Gd_{0.1}Y_{0.1}O_3- \delta$ (BSCZGY): a case study on effect of sintering temperature**.** *Journal of the American Ceramic Society* **2016**, 9, 866-875.

[42] Michiura, N.; Tatekawa, T.; Higuchi, Y.; Tamura, H. Role of donor and acceptor ions in the dielectric loss tangent of $(Zr_{0.8}Sn_{0.2})TiO_4$ dielectric resonator material**.** *Journal of the American Ceramic Society* **1995**, 78, 793-796

[43] Guo, F.; Wu, X.; Lu, Q.; Zhao, S. Near room temperature giant negative and positive electrocaloric effects coexisting in lead–free $BaZr_{0.2}Ti_{0.8}O_3$ relaxor ferroelectric films. *Ceramics International* **2018**, 44, 2803-2808.

[44] Wu, L.; Chen, Y.C.; Chou, Y.P.; Tsai, Y.T.; Chu, S.Y. Dielectric properties of Al_2O_3−doped barium strontium titanate for application in phased array antennas; *Japanese Journal of Applied Physics* **1999**, 38, 5154-5161.

[45] Lahiry, S.; Mansingh, A. Sol-Gel Derived $Ba_x Sr_{1-x}TiO_3$ Films for Microwave Applications. *Ferroelectrics* **2005**, 329, 39-42.

Figures Captions

Figure 1

RMS – root mean square; BZT – barium zirconium titanate; x – zirconium content; nm – nanometers; µm – micrometers; AFM – atomic force microscopy.

Figure 1: 2 µm x 2 µm surface AFM images of BZT thin films with different zirconium contents.

Images taken on the films surface show granular films with clear differences between the morphologies of their surfaces. Root mean square (RMS) roughness values decrease with the zirconium content increase due to the gradual decrease in grain size since the barium zirconate ($BaZrO_3$) is a difficult refractory oxide (T_{fusion} =2600 °C).

Figure 2

RMS – root mean square; nm – nanometers; Zr – zirconium; BZT – barium zirconium titanate; AFM – atomic force microscopy.

Figure 2: BZT thin films roughness measured by AFM microscopy as a function of zirconium content.

Root mean square (RMS) roughness values decrease with the zirconium content increase due to the slow diffusion of the Zr^{4+} ion of larger ionic radius than that of Ti^{4+} ion. As a first approximation, the measured BZT thin films roughness is almost linear as a function of zirconium content starting from x=0.15, which could make possible the surface roughness control by adjusting the Ti/Zr ratio.

Figure 3

x – zirconium content ; V – Volt ; (°) – degree ; BZT – barium zirconium titanate ; BZT0.05 – BZT thin film with x = 0.05 ; BZT0.15 – BZT thin film with x = 0.15 ; BZT0.25 – BZT thin film with x = 0.25 ; BZT0.35 – BZT thin film with x = 0.35.

Figure 3: Local piezoelectric hysteresis loops phase-recorded at a grain of BZT0.05 (a), BZT0.15 (b), BZT0.25 (c) and BZT0.35 (d) thin films.

The phase gives information about the direction of the mechanical variation of the grain under a DC voltage. Well-defined hysteresis loops are obtained for all compositions under the applied electric field excitation. Loops are more inclined as the zirconium rate increases since the material tends to become paraelectric for x higher than 0.35 at room temperature. Local piezoelectric phase responses also degrade: from 140° for x=0.05 to 120° for x=0.35 for phase difference. Asymmetry observed over the loops due to the shift to positive or negative values of the applied voltage is attributed to the internal electric field at the film/electrode interface or the tip/film/electrode system.

Figure 4

x – zirconium content ; V – Volt ; BZT – barium zirconium titanate ; BZT0.05 – BZT thin film with x = 0.05 ; BZT0.15 – BZT thin film with x = 0.15 ; BZT0.25 – BZT thin film with x = 0.25 ; BZT0.35 – BZT thin film with x = 0.35.

Figure 4: local amplitude recorded loops at the center of individual grains of BZT0.05 (a), BZT0.15 (b), BZT0.25 (c) and BZT0.35 (d) thin films.

The measured amplitude defines the local electromechanical response of the grain under a DC voltage owing the converse piezoelectric effect. The amplitude decreases from 0.8 mV for x=0.05 to 0.25 mV for x=0, showing that the BZT thin films piezoelectric character decreases with increasing zirconium content in the composition. The butterfly-wing appearance of the curves confirms the ferroelectric and piezoelectric character of BZT grains. Observed

differences in the amplitude variations for positive and negative polarization may be due to the interface effect and/or the instrumental electrostatic contribution.

Figure 5-a

x – zirconium content ; V – Volt ; BZT – barium zirconium titanate ; a.u. – arbitrary units; A – amplitude; φ – phase.

Figure 5-a: Acosφ piezoelectric response recorded at a grain of BZT thin films with $x \leq 0.25$.

Typical piezoelectric loops of a ferroelectric material are obtained for BZT thin films with $x<0.25$. The width of the loops decreases as the zirconium content increases. The low hysteresis loop opening observed for x=0.25 shows that the ferroelectric to paraelectric transition of this film is very close to room temperature, at which the measurements were made.

Figure 5-b

x – zirconium content ; V – Volt ; BZT – barium zirconium titanate ; a.u. – arbitrary units; A – amplitude; φ – phase.

Figure 5-b: Acosφ piezoelectric response recorded at a grain of BZT thin films with $x \geq 0.25$

Acosφ piezoelectric response show that the room temperature is very close to the ferroelectric to paraelectric transition for x=0.25 as the hysteresis loop is very little open. Nevertheless, for $x \geq 0.3$ no hysteresis loop is observed, which shows that for these compositions BZT films are in the paraelectric state at room temperature.

Figure 6

ε' – dielectric permittivity; x – zirconium content ; BZT – barium zirconium titanate.

Figure 6: Frequency dependence of the BZT thin films dielectric permittivity ε' at room temperature.

The dielectric constant is very sensitive to stoichiometry with for each composition, a slight decrease of 7% to 13% in the range [1 kHz-1 MHz]. This decrease is due to oxygen gaps,

extrinsic effects such as electrode interface effects and impurities and also to the dipoles that could not follow the rapidly alternation of the electric field in the whole frequency range.

Figure 7

ε' – dielectric permittivity; x – zirconium content ; BZT – barium zirconium titanate; Zr (%) – zirconium percentage; MHz – Megahertz.

Figure 7: BZT thin films dielectric permittivity ε' as a function of zirconium content at 1 MHz and room temperature.

The dielectric constant increases and passes through a maximum for a zirconium content of 10% and then gradually decreases with the zirconium content increasing. The maximum value is obtained for x=0.1 as the Curie temperature for this composition is close to room temperature at which measurements are made. For higher zirconium contents, the paraelectric-ferroelectric transition temperature decreases, resulting in a decrease in dielectric permittivity.

Figure 8

tgδ – dielectric loss tangent; x – zirconium content ; BZT – barium zirconium titanate.

Figure 8: Frequency dependence of the BZT thin films dielectric loss tangent tgδ at room temperature.

High losses observed at low frequencies are due to space charges polarization losses attributed to the macroscopic movement of charge carriers captured by defects, impurity, phase boundary, etc… The dielectric loss tangent tgδ gradually decreases with frequency increasing, except for x=0.05 due to a possible dielectric relaxation to be confirmed by measurements beyond 1 MHz. A slight dielectric relaxation is noted for x=0.1 and x=0.2.

Figure 9

ε'' – dielectric losses; tgδ – dielectric loss tangent; x – zirconium content ; BZT – barium zirconium titanate; Zr (%) – zirconium percentage; MHz – Megahertz.

Figure 9: BZT thin films dielectric losses ε'' and dielectric loss tangent tgδ as a function of zirconium content at 1 MHz and room temperature.

Dielectric losses increase and go through a maximum for a zirconium rate of 10% and then decrease, in the same way as the dielectric constant evolution. The maximum value is obtained for x=0.1 as the Curie temperature for this composition is close to room temperature at which measurements are made. The dielectric loss tangent continuously decreases with the zirconium content increase: $tg\delta_{min} = 1.4\ 10^{-2}$ for x=0.35 at 1 MHz, which is interesting for electronic applications.

Figure 10

ε' – dielectric permittivity; x – zirconium content; BZT – barium zirconium titanate; Zr – zirconium; E – electric field; V – Volt; cm – centimeter; MHz – Megahertz.

Figure 10: BZT thin films dielectric permittivity ε' as a function of the applied electric field for different zirconium contents at 1 MHz and room temperature.

The observed "butterfly wing" shape on the curves attests to the BZT thin films ferroelectric behavior. The highest dielectric permittivity values are obtained for x=0.1 as expected. The hysteresis effect decreases with the zirconium content increasing, as more x increases, the closer the material gets to the paraelectric state at room temperature. Nevertheless, the "butterfly-wing" shape is still present up to x=0.35.

Figure 11

ε'' – dielectric losses; x – zirconium content; BZT – barium zirconium titanate; Zr – zirconium; E – electric field; V – Volt; cm – centimeter; MHz – Megahertz.

Figure 11: BZT thin films dielectric losses ε'' as a function of the applied electric field for different Zr contents at 1 MHz and room temperature.

Dielectric losses show a "butterfly wing" shape indicating the BZT thin films ferroelectric behavior. The highest dielectric losses values are obtained for x=0.1 as expected. Dielectric

losses nonlinearly decrease with the electric field increasing, due to the anharmonic interaction of Ti ions at the paraelectric phase. This shows that such samples have a very good resistance to breakdown.

Figure 12

x – zirconium content; BZT – barium zirconium titanate; Zr – zirconium; E – electric field; V – Volt; cm – centimeter; MHz – Megahertz.

Figure 12: BZT thin films tunability as a function of the applied electric field for different Zr contents at 1 MHz and room temperature.

The tunability increases monotonically as the applied electric field increases for all the BZT thin films compositions. The highest tunability is achieved for the BZT0.1 thin film, which has the highest dielectric permittivity and dielectric losses at room temperature.

Figure 13

x – zirconium content; BZT – barium zirconium titanate; Zr – zirconium; E – electric field; V – Volt; cm – centimeter; MHz – Megahertz.

Figure 13: BZT thin films tunability as a function of Zr content at 1 MHz, 240 kV/cm and room temperature.

The tunability increases with the zirconium content increasing, passes through a maximum of 32% at 240 kV/cm and 1 MHz for x=0.1 at room temperature, then decreases. The composition with the highest tunability is indeed the one for which the ferroelectric-to-paraelectric phase transition temperature is the closest to room temperature at which measurements are made.

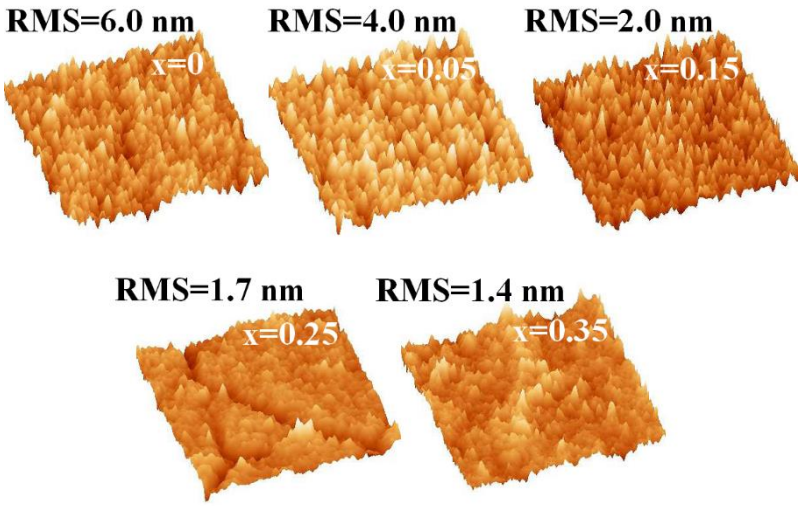

Figure 1: 2 µm x 2 µm surface AFM images of BZT thin films with different zirconium contents. RMS – root mean square; BZT – barium zirconium titanate; x – zirconium content; nm – nanometers; µm – micrometers; AFM – atomic force microscopy.

Images taken on the films surface show granular films with clear differences between the morphologies of their surfaces. Root mean square (RMS) roughness values decrease with the zirconium content increase due to the gradual decrease in grain size since the barium zirconate ($BaZrO_3$) is a difficult refractory oxide (T_{fusion} =2600 °C).

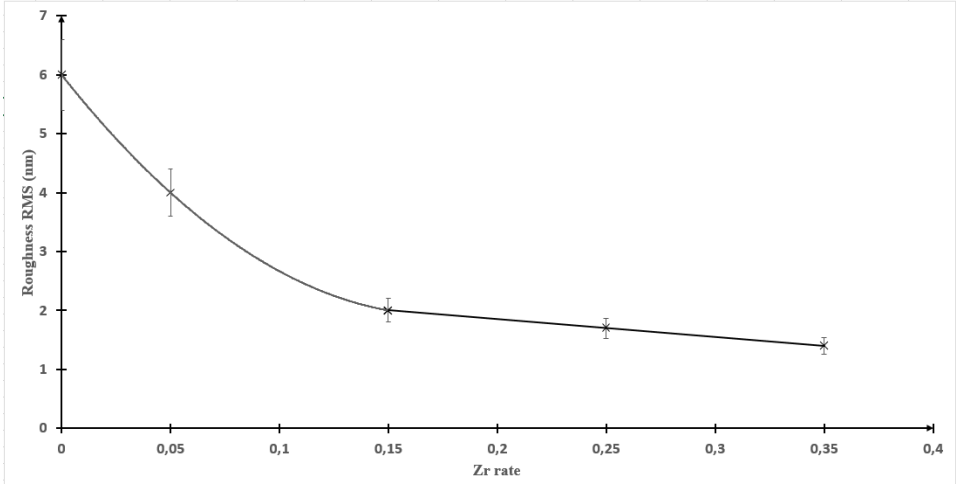

Figure 2: BZT thin films roughness measured by AFM microscopy as a function of zirconium content. RMS – root mean square; nm – nanometers; Zr – zirconium; BZT – barium zirconium titanate; AFM – atomic force microscopy.

Root mean square (RMS) roughness values decrease with the zirconium content increase due to the slow diffusion of the Zr^{4+} ion of larger ionic radius than that of Ti^{4+} ion. As a first approximation, the measured BZT thin films roughness is almost linear as a function of zirconium content starting from x=0.15, which could make possible the surface roughness control by adjusting the Ti/Zr ratio.

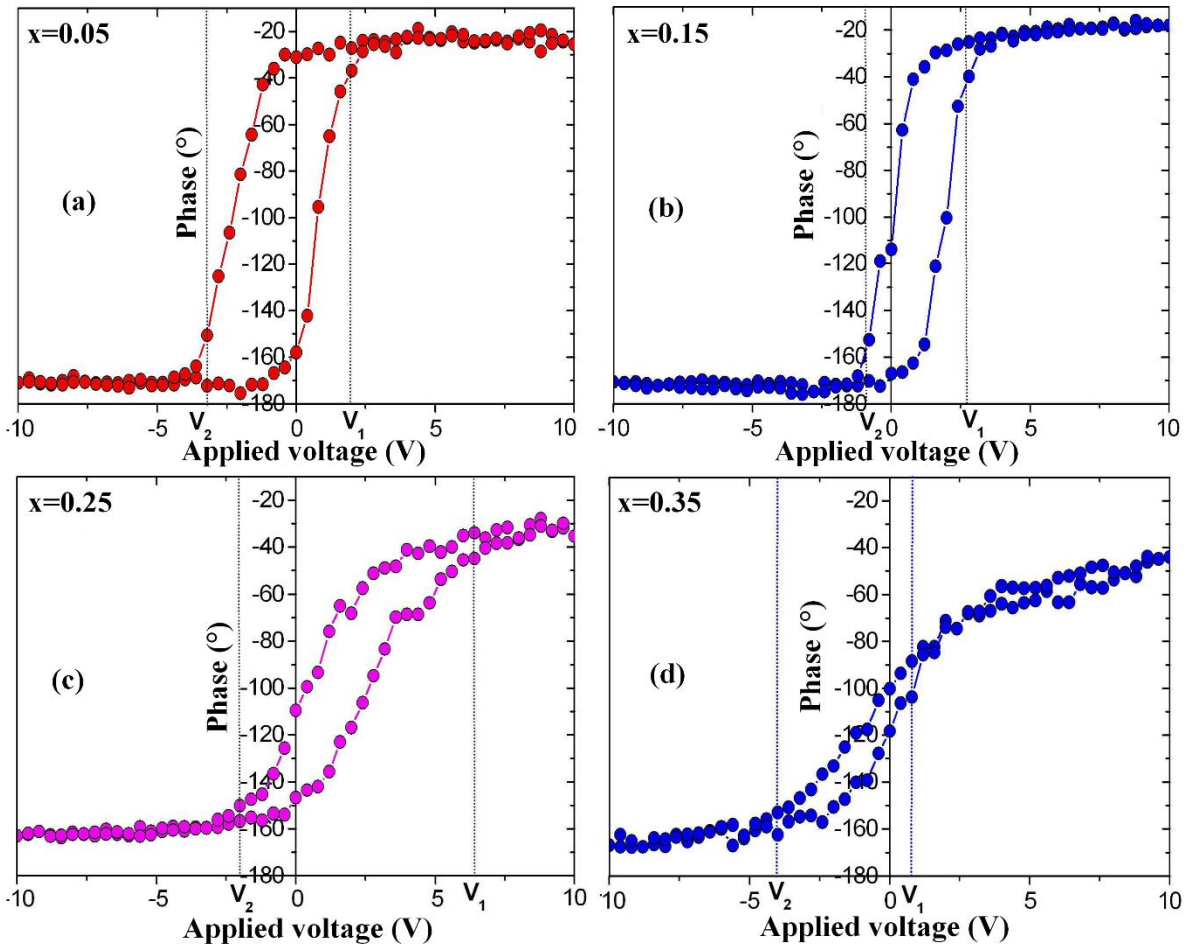

Figure 3: Local piezoelectric hysteresis loops phase-recorded at a grain of BZT0.05 (a), BZT0.15 (b), BZT0.25 (c) and BZT0.35 (d) thin films. x – zirconium content ; V – Volt ; (°) – degree ; BZT – barium zirconium titanate ; BZT0.05 – BZT thin film with x = 0.05 ; BZT0.15 – BZT thin film with x = 0.15 ; BZT0.25 – BZT thin film with x = 0.25 ; BZT0.35 – BZT thin film with x = 0.35.

The phase gives information about the direction of the mechanical variation of the grain under a DC voltage. Well-defined hysteresis loops are obtained for all compositions under the applied electric field excitation. Loops are more inclined as the zirconium rate increases since the material tends to become paraelectric for x higher than 0.35 at room temperature. Local piezoelectric phase responses also degrade: from 140° for x=0.05 to 120° for x=0.35 for phase difference. Asymmetry observed over the loops due to the shift to positive or negative values of the applied voltage is attributed to the internal electric field at the film/electrode interface or the tip/film/electrode system.

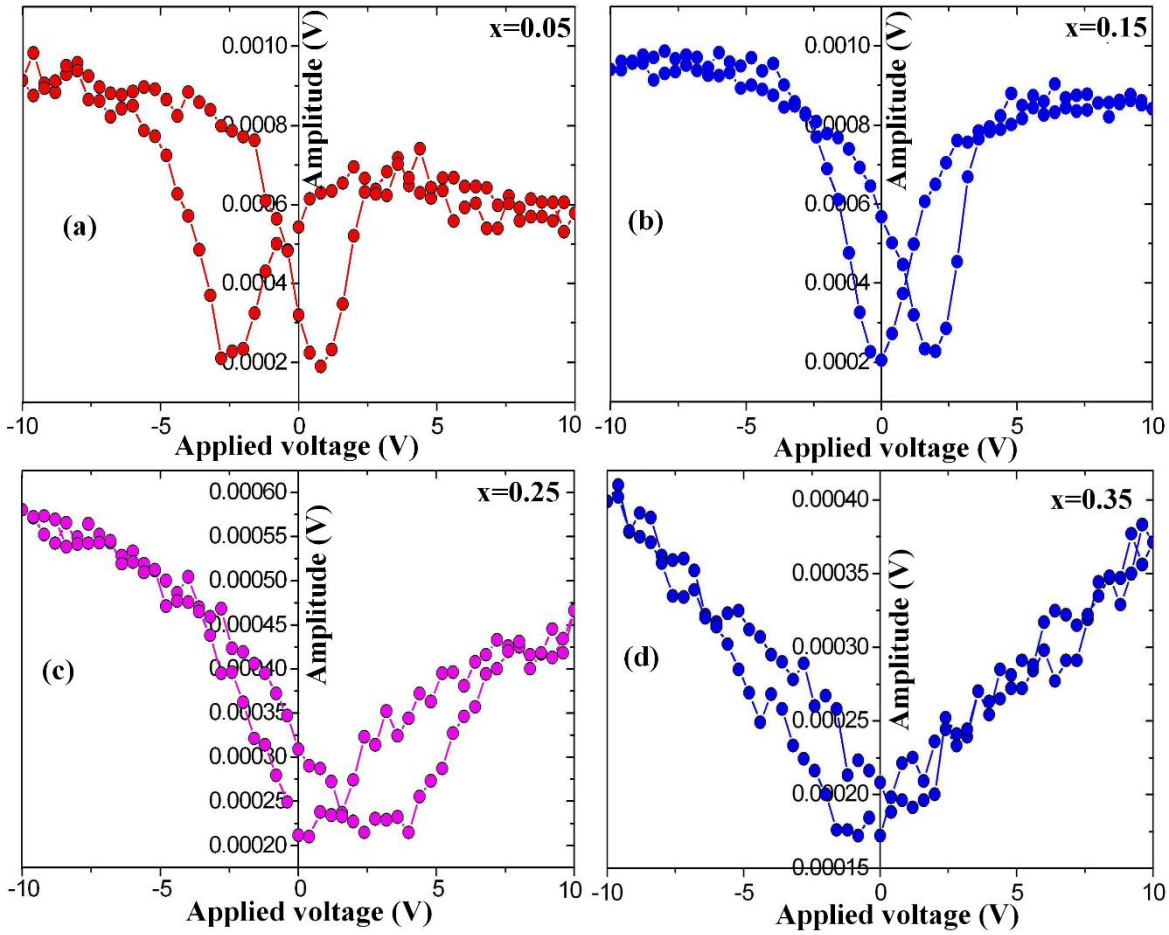

Figure 4: local amplitude recorded loops at the center of individual grains of BZT0.05 (a), BZT0.15 (b), BZT0.25 (c) and BZT0.35 (d) thin films. x – zirconium content ; V – Volt ; BZT – barium zirconium titanate ; BZT0.05 – BZT thin film with x = 0.05 ; BZT0.15 – BZT thin film with x = 0.15 ; BZT0.25 – BZT thin film with x = 0.25 ; BZT0.35 – BZT thin film with x = 0.35.

The measured amplitude defines the local electromechanical response of the grain under a DC voltage owing the converse piezoelectric effect. The amplitude decreases from 0.8 mV for x=0.05 to 0.25 mV for x=0, showing that the BZT thin films piezoelectric character decreases with increasing zirconium content in the composition. The butterfly-wing appearance of the curves confirms the ferroelectric and piezoelectric character of BZT grains. Observed differences in the amplitude variations for positive and negative polarization may be due to the interface effect and/or the instrumental electrostatic contribution.

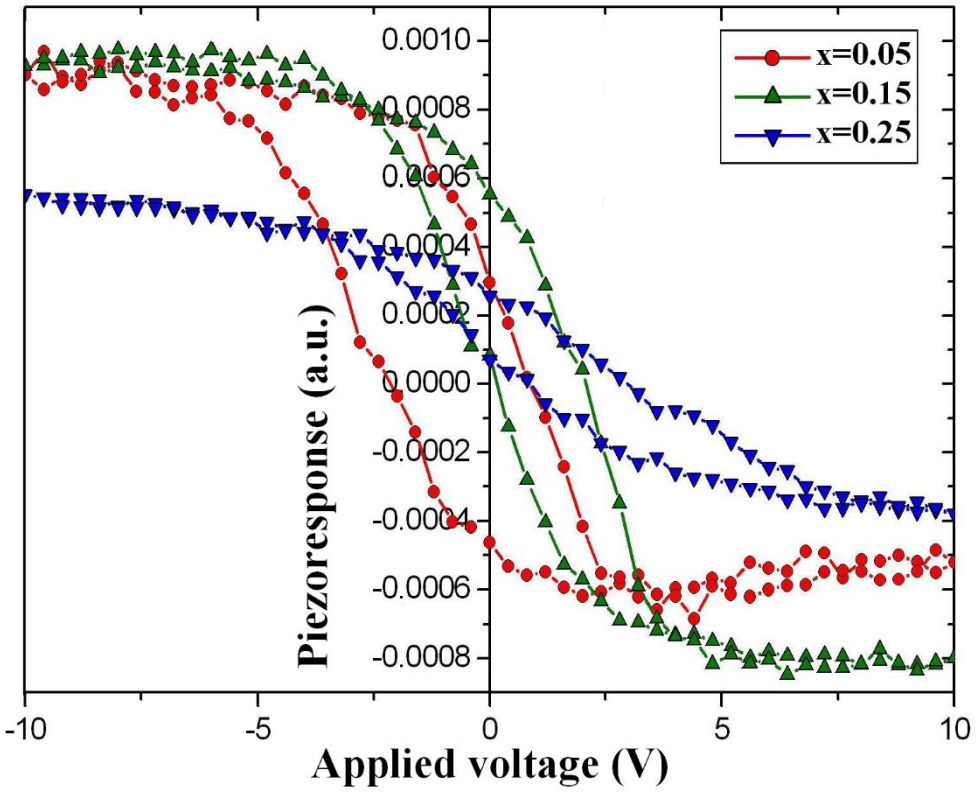

Figure 5-a: Acosφ piezoelectric response recorded at a grain of BZT thin films with $x \leq 0.25$. x – zirconium content ; V – Volt ; BZT – barium zirconium titanate ; a.u. – arbitrary units; A – amplitude; φ – phase.

Typical piezoelectric loops of a ferroelectric material are obtained for BZT thin films with $x<0.25$. The width of the loops decreases as the zirconium content increases. The low hysteresis loop opening observed for x=0.25 shows that the ferroelectric to paraelectric transition of this film is very close to room temperature, at which the measurements were made.

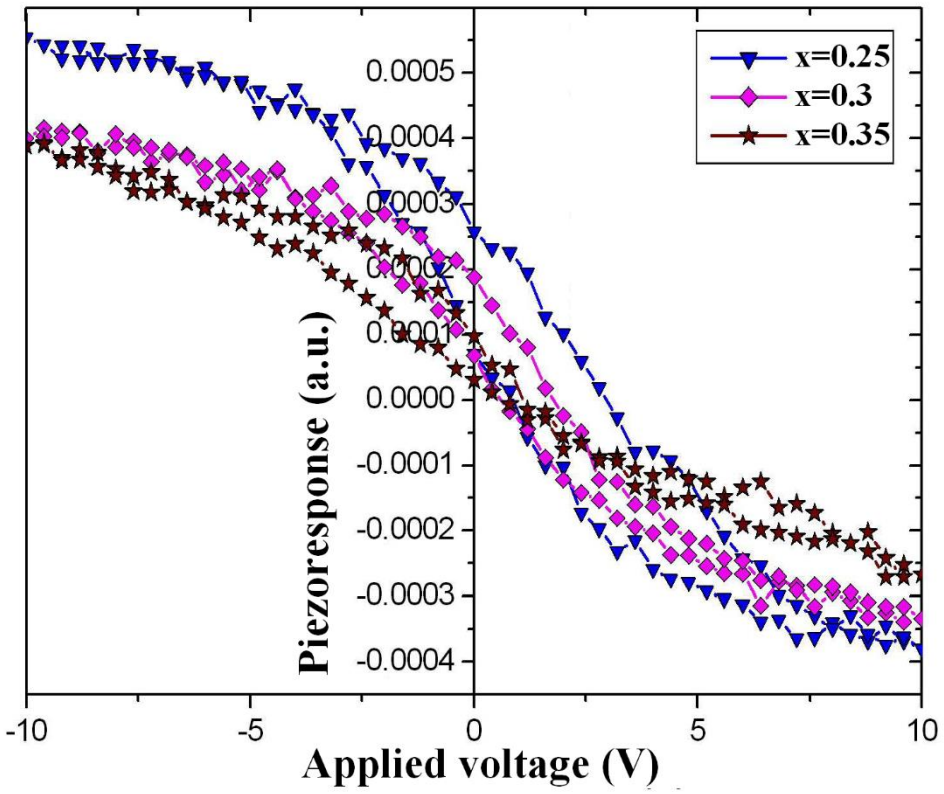

Figure 5-b: Acosφ piezoelectric response recorded at a grain of BZT thin films with x ≥ 0.25. x – zirconium content ; V – Volt ; BZT – barium zirconium titanate ; a.u. – arbitrary units; A – amplitude; φ – phase.

Acosφ piezoelectric response show that the room temperature is very close to the ferroelectric to paraelectric transition for x=0.25 as the hysteresis loop is very little open. Nevertheless, for x≥0.3 no hysteresis loop is observed, which shows that for these compositions BZT films are in the paraelectric state at room temperature.

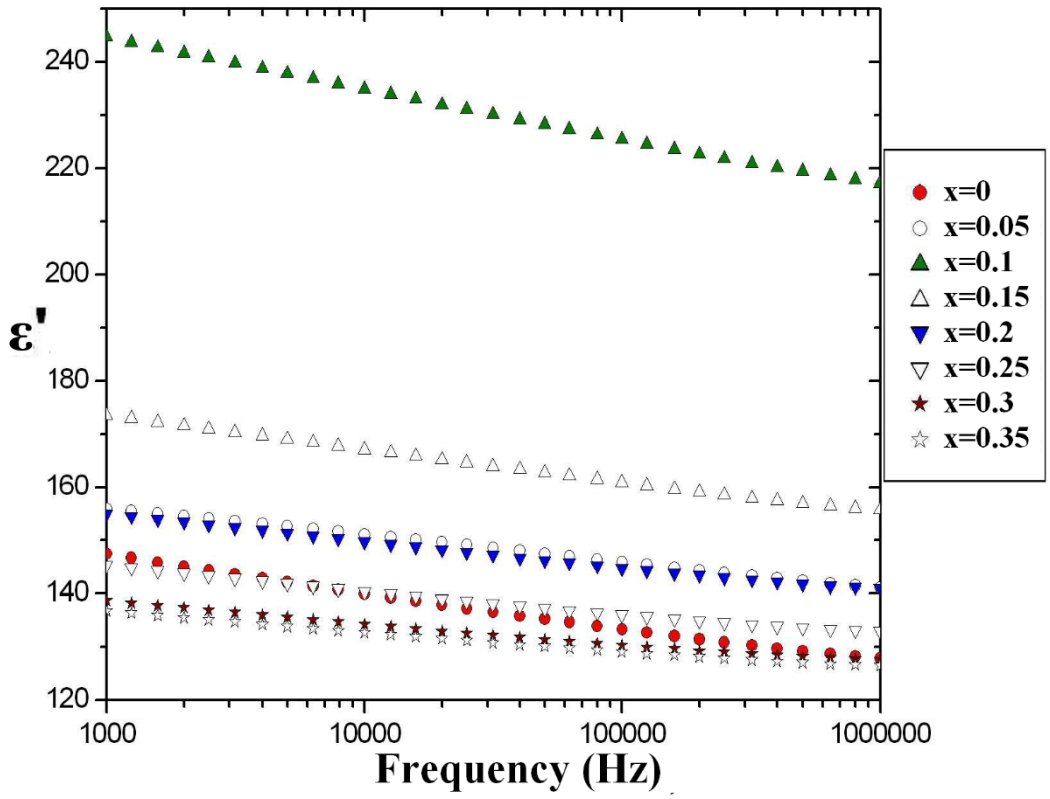

Figure 6: Frequency dependence of the BZT thin films dielectric permittivity ε' at room temperature. **ε'** – dielectric permittivity; x – zirconium content ; BZT – barium zirconium titanate.

The dielectric constant is very sensitive to stoichiometry with for each composition, a slight decrease of 7% to 13% in the range [1 kHz-1 MHz]. This decrease is due to oxygen gaps, extrinsic effects such as electrode interface effects and impurities and also to the dipoles that could not follow the rapidly alternation of the electric field in the whole frequency range.

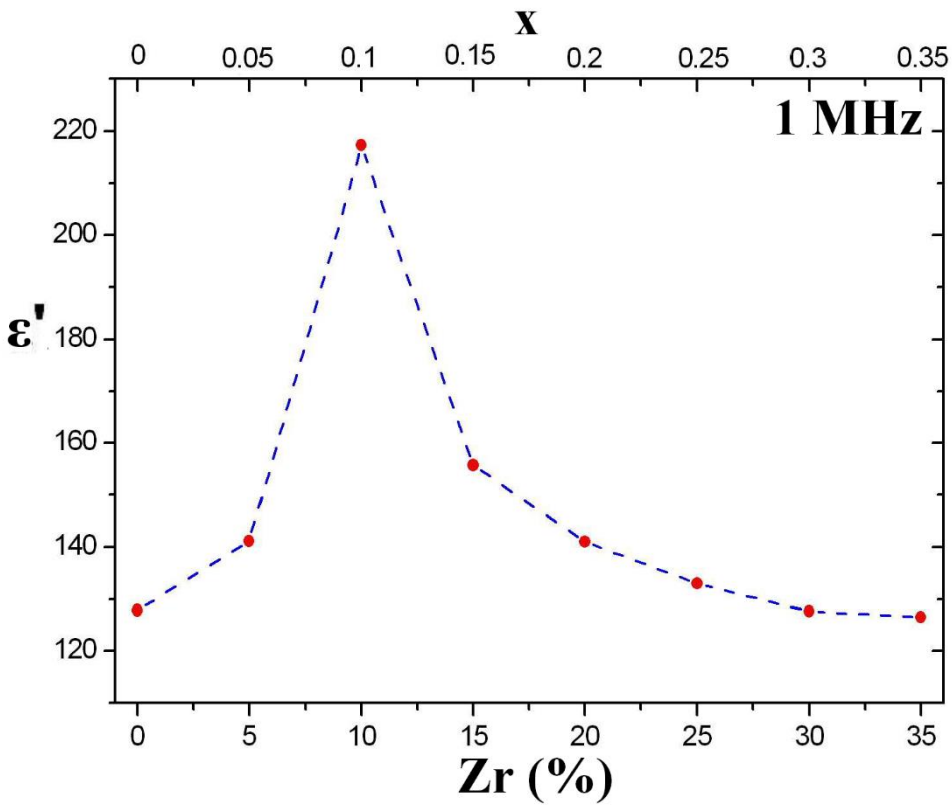

Figure 7: BZT thin films dielectric permittivity ε' as a function of zirconium content at 1 MHz and room temperature. **ε'** – dielectric permittivity; x – zirconium content ; BZT – barium zirconium titanate; Zr (%) – zirconium percentage; MHz – Megahertz.

The dielectric constant increases and passes through a maximum for a zirconium content of 10% and then gradually decreases with the zirconium content increasing. The maximum value is obtained for x=0.1 as the Curie temperature for this composition is close to room temperature at which measurements are made. For higher zirconium contents, the paraelectric-ferroelectric transition temperature decreases, resulting in a decrease in dielectric permittivity.

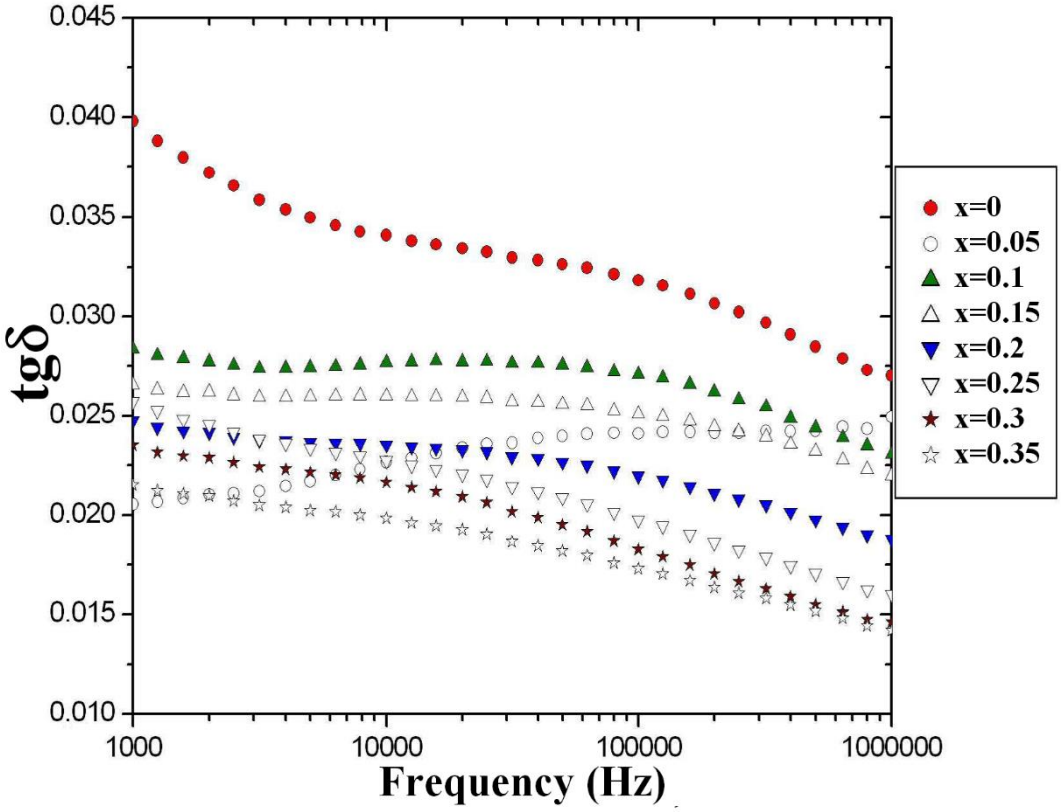

Figure 8: Frequency dependence of the BZT thin films dielectric loss tangent tgδ at room temperature. tgδ – dielectric loss tangent; x – zirconium content ; BZT – barium zirconium titanate.

High losses observed at low frequencies are due to space charges polarization losses attributed to the macroscopic movement of charge carriers captured by defects, impurity, phase boundary, etc… The dielectric loss tangent tgδ gradually decreases with frequency increasing, except for x=0.05 due to a possible dielectric relaxation to be confirmed by measurements beyond 1 MHz. A slight dielectric relaxation is noted for x=0.1 and x=0.2.

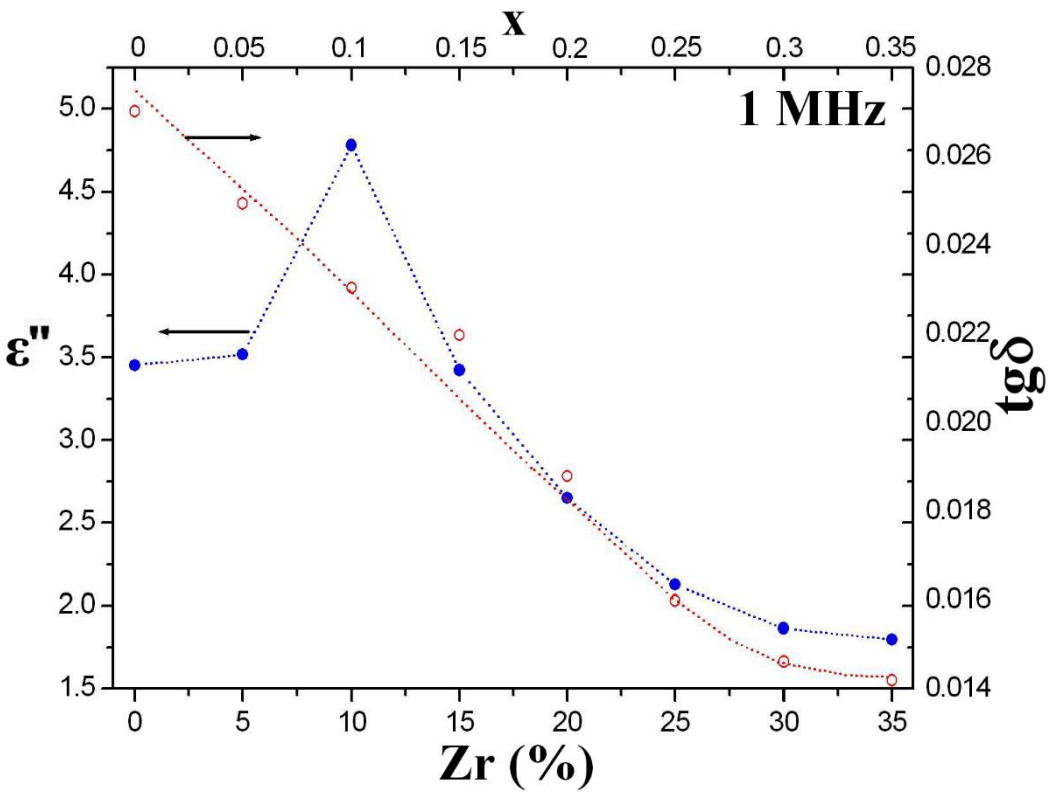

Figure 9: BZT thin films dielectric losses ε'' and dielectric loss tangent tgδ as a function of zirconium content at 1 MHz and room temperature. ε'' – dielectric losses; tgδ – dielectric loss tangent; x – zirconium content ; BZT – barium zirconium titanate; Zr (%) – zirconium percentage; MHz – Megahertz.

Dielectric losses increase and go through a maximum for a zirconium rate of 10% and then decrease, in the same way as the dielectric constant evolution. The maximum value is obtained for x=0.1 as the Curie temperature for this composition is close to room temperature at which measurements are made. The dielectric loss tangent continuously decreases with the zirconium content increase: $tg\delta_{min} = 1.4\ 10^{-2}$ for x=0.35 at 1 MHz, which is interesting for electronic applications.

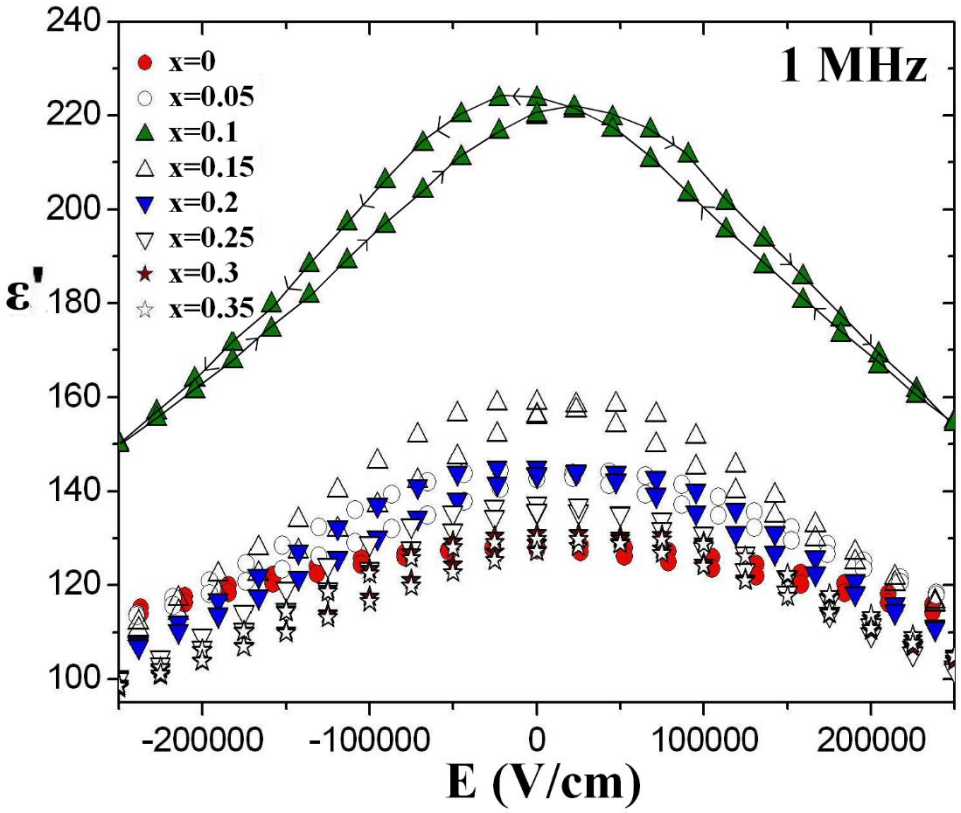

Figure 10: BZT thin films dielectric permittivity ε' as a function of the applied electric field for different zirconium contents at 1 MHz and room temperature. **ε'** – dielectric permittivity; x – zirconium content; BZT – barium zirconium titanate; Zr – zirconium; E – electric field; V – Volt; cm – centimeter; MHz – Megahertz.

The observed "butterfly wing" shape on the curves attests to the BZT thin films ferroelectric behavior. The highest dielectric permittivity values are obtained for x=0.1 as expected. The hysteresis effect decreases with the zirconium content increasing, as more x increases, the closer the material gets to the paraelectric state at room temperature. Nevertheless, the "butterfly-wing" shape is still present up to x=0.35.

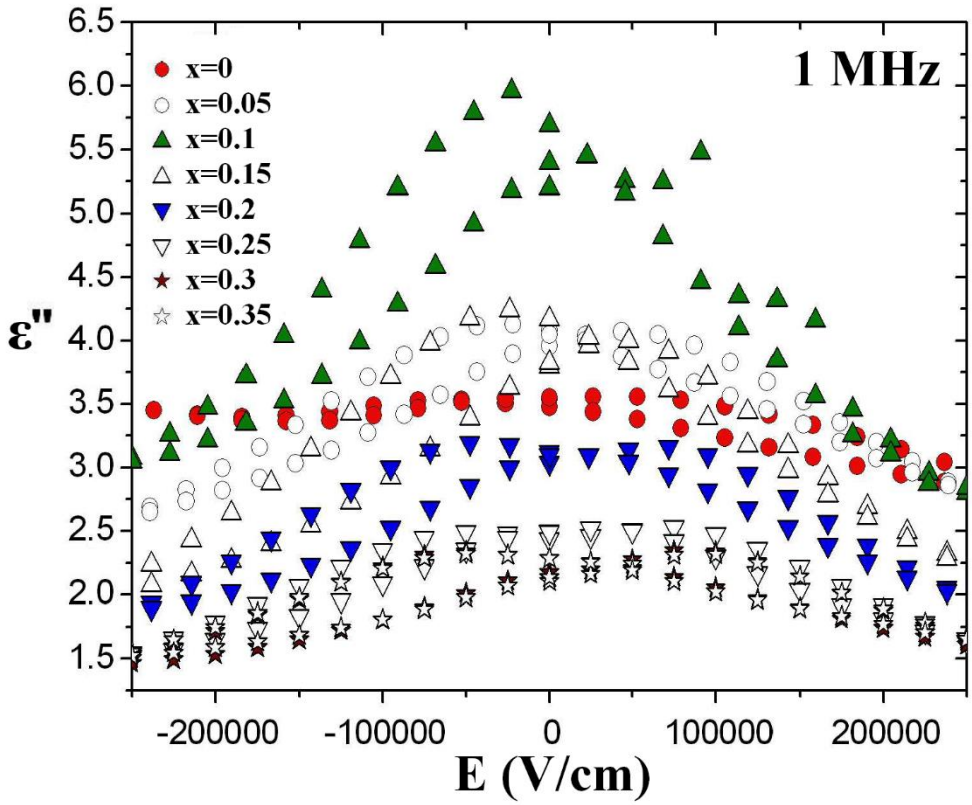

Figure 11: BZT thin films dielectric losses ε'' as a function of the applied electric field for different Zr contents at 1 MHz and room temperature. ε'' – dielectric losses; x – zirconium content; BZT – barium zirconium titanate; Zr – zirconium; E – electric field; V – Volt; cm – centimeter; MHz – Megahertz.

Dielectric losses show a "butterfly wing" shape indicating the BZT thin films ferroelectric behavior. The highest dielectric losses values are obtained for x=0.1 as expected. Dielectric losses nonlinearly decrease with the electric field increasing, due to the anharmonic interaction of Ti ions at the paraelectric phase. This shows that such samples have a very good resistance to breakdown.

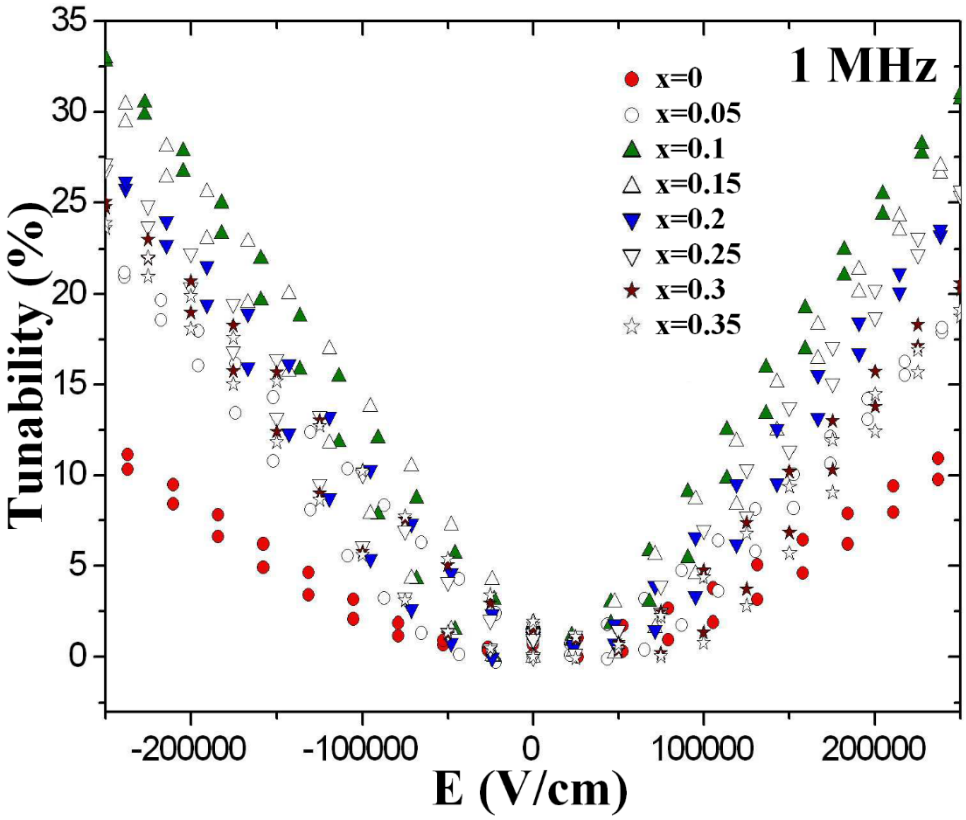

Figure 12: BZT thin films tunability as a function of the applied electric field for different Zr contents at 1 MHz and room temperature. x – zirconium content; BZT – barium zirconium titanate; Zr – zirconium; E – electric field; V – Volt; cm – centimeter; MHz – Megahertz.

Figure 12: BZT thin films tunability as a function of the applied electric field for different Zr contents at 1 MHz and room temperature.

The tunability increases monotonically as the applied electric field increases for all the BZT thin films compositions. The highest tunability is achieved for the BZT0.1 thin film, which has the highest dielectric permittivity and dielectric losses at room temperature.

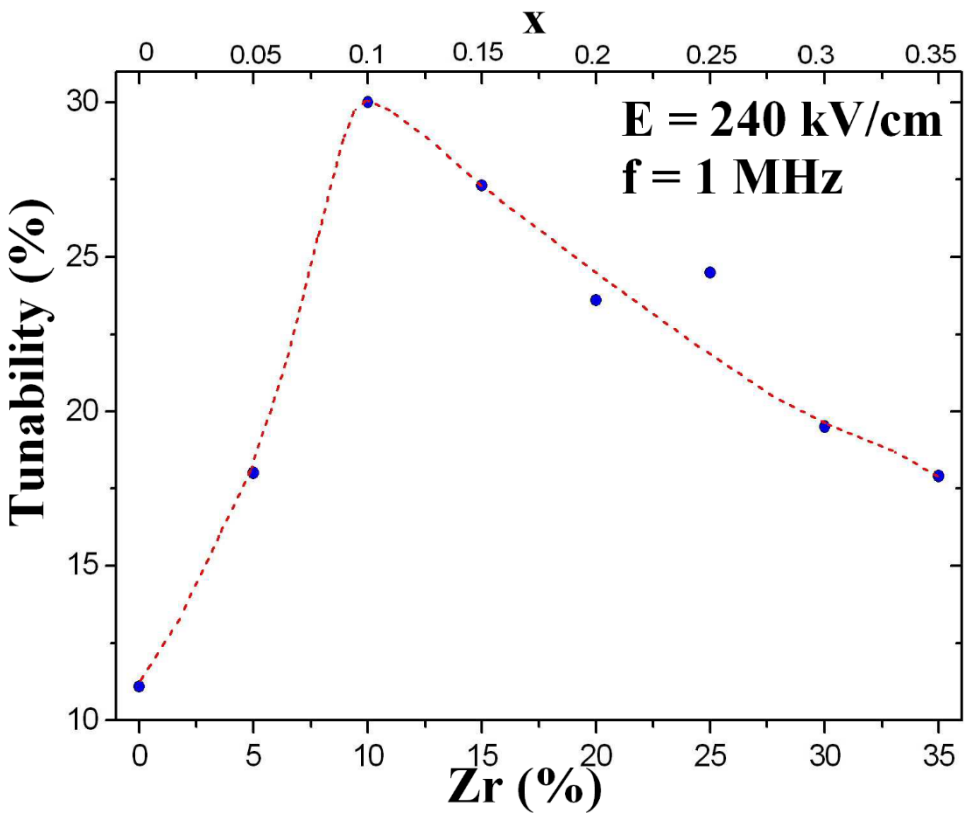

Figure 13: BZT thin films tunability as a function of Zr content at 1 MHz, 240 kV/cm and room temperature. x – zirconium content; BZT – barium zirconium titanate; Zr – zirconium; E – electric field; V – Volt; cm – centimeter; MHz – Megahertz.

The tunability increases with the zirconium content increasing, passes through a maximum of 32% at 240 kV/cm and 1 MHz for x=0.1 at room temperature, then decreases. The composition with the highest tunability is indeed the one for which the ferroelectric-to-paraelectric phase transition temperature is the closest to room temperature at which measurements are made.